IRAQI JOURNAL OF APPLIED PHYSICS
Vol. 22, No. 1, January-March 2026, pp. 82-90

Hassein A. Hassein [1,2*]
Ali Q. Abdullah [2]
Widad S. Hanoosh [2]

[1] Department of Physics, College of Science, University of Basrah, Basrah, IRAQ
[2] Department of Medical Physics, College of Medical Science, Jabir Ibn Hayan University, Kufa, IRAQ
*Corresponding author: bondshamsuldeen@gmail.com

Optical Properties of Polyvinyl Pyridine Fibers (PVP) Prepared by Electrospinning

In this study, polyvinylpyrrolidone (PVP) nanofibers were synthesized using the electrospinning technique. The findings indicate that key process parameters, including applied voltage, polymer concentration, collecting distance, drum rotation speed, and flow rate, significantly influence fiber formation. These parameters played a crucial role in minimizing fiber diameter. This experimental investigation provides a comprehensive analysis of the impact of various electrospinning conditions on the fabrication of PVP nanofibers, contributing to a deeper understanding of the optimization of fiber morphology and properties. The structural and morphological characteristics of the PVP nanofibers were analyzed using X-ray diffraction (XRD) and scanning electron microscopy (SEM) techniques. Beyond examining fiber diameter, this research investigates how variations in electrospinning parameters influence the structural, thermal, and optical properties of PVP nanofibers The optical properties of the PVP nanofiber thin films were examined through transmission and absorption spectra measured at room temperature over the wavelength range of 300–900 nm. The optical energy gap ((E_o = 3.98 eV)) and other related parameters were determined using Tauc's relation.

Keywords: Electrospinning; Polyvinylpyrrolidone; Optical energy gap; Fiber diameter
Received: 27 April 2025; Revised: 23 July 2025; Accepted: 30 July 2025; Published: 1 January 2026

1. Introduction

One well-known and simple technique for creating nanofibers from a variety of materials, including metals, polymers, and ceramics, is electrospinning. When a large electric field is present during the procedure, the polymer solution stretches, producing micro- and nanoscale fibers [1,2]. This approach produces electrospun nanofibers with exceptional properties, making them highly suitable for various industrial applications. These properties include high porosity, flexibility, and a large surface area-to-volume ratio, and superior aspect ratio. Tissue engineering, filtration, health and personal care, sensors, energy harvesting, sound absorption, and storage are a few of these uses [3,4]. The electrospinning technique entails applying an electric charge to the polymer solution, which causes the solution jet to stretch in a strong electric field, resulting in the production of nanofibers. Thus, the polymer solution elongates and stretches into the Taylor cone - a conical shape - when it flows out of the needle that is attached to a high-voltage DC power source. At this time, the conical droplet crosses the surface tension with a rising electric field, and the electrostatic force created causes the charged polymer jet to extrude out in the form of fibers. Due to the opposing charge, the thin stretched fibers move more quickly in the direction of the collector end and gather there to create fiber networks [5-7]. The electrospinning process involves several factors that influence the shape of the nanofiber. The parameters are divided into three categories: (a) the electrospinning process is influenced by various factors, including (a) processing parameters such as applied voltage, solution flow rate, needle-to-collector distance, needle tip design, collector geometry, and velocity; (b) solution properties, including concentration, viscosity, surface tension, molecular weight, and solvent type; and (c) environmental conditions such as temperature and humidity. By carefully adjusting and optimizing these electrospinning parameters, the desired fiber morphology can be effectively achieved [8,9]. Many academics have looked at the impact of these characteristics on fiber geometry in various research. The most significant component influencing the fiber shape and diameter values is the concentration, which may be changed to control the viscosity of the polymer solution. Shivkumar and Tao [10] have studied the impact of molecular weight on fiber morphology was investigated using PVA. Spray patterns and beads were generated at lower concentrations of 7–16 wt.%, as they observed. Concentrations over 24 wt.% produced a ribbon-like structure, whereas concentrations below 22 wt.% produced homogenous and smooth nanofibers. Deitzel et al. [11] have examined the impact of varying concentrations of polyethylene oxide (PEO) (from 4 to 10 wt.%) on the fiber diameter and found that greater concentration led to an increase in fiber diameter. Koski et al. [12] have found that the concentration of PEO electrospun nanofibers depends on their fiber diameter. They also looked at the significant change in diameter that occurred as the voltage changed [13]. Yuantal and Kattietal asserted that due of the increased electrostatic repulsive forces, the higher voltages aid in the production of smaller fibers. Thus, it was shown that although the fiber diameter is dependent on voltage, the effect is negligible in comparison to the polymer concentration. In addition to analyzing fiber diameter, this study explores the influence of different

electrospinning parameters on the structural, thermal, and optical features of PVP-based nanofibers. Another crucial component that influences the jet's velocity and fiber diameter is the flow rate [14-16]. The following factors affect the fiber properties. High voltage, as the fiber diameter value drops as a result of the polymer solution stretching more when voltage is applied [15]. The solvent will evaporate faster at a higher voltage, drying it off earlier [17,18]. Shorter flash periods for the polymer jet at lower voltage levels increase the possibility of smoother fibers [19].

Solution concentration is also affecting factor as the greater concentration of polymer solution results in an increase in the fiber diameter value. Defects begin to show up on the nanofiber mat as beads at decreasing concentrations. The potential for electrospraying also rises at lower concentrations [8,12].

Rotational velocity is affecting as well. When a stationary rotor is used instead of a spinning collector, the average fiber diameter value is larger. The diameter of the fibers drops as the rotating collector RPM increases, however the value decrease is not statistically significant [20].

Collecting distance is an affecting factor as well as the fibers will get more stretched and extended as the distance and duration of flight increase [19]. Beads begin to emerge where the needle and collector are more apart. Bead formation also occurs at smaller distances because the polymer jet does not have enough time to solidify [21,22]. To get smooth fibers, the ideal distance is necessary [15].

Flow rate is an important factor since a reduced flow rate of polymer solution gives the fibers more time to stretch, the fiber diameter decreases [15]. As the fibers' drying time decreases, higher flow rate values produce thicker fibers containing. The production of fibers using electrospinning is a multifaceted process wherein several factors impact the diameter and shape of the fibers. To produce the necessary tiny smooth/finite nanofibers without beads, further research has to be done on the association between these characteristics and the corresponding fiber geometries. Researchers have attempted to model the process several times, however only a small number of variables are included in these studies [22].

In this study, the effect of factors on the diameters of fibers prepared from PVP prepared using the electrospinning method (the electric field strength, polymer solution concentration, feed rate, and rotational speed of the collector drum) was studied. The optical properties of nanofibers films prepared were studied, and some optical constants were calculated, including the optical energy gap.

2. Experimental Details

The polymer polyvinylpyrrolidone (PVP) with an average molecular weight K-value (K=90) of $1.3x10^6$ g/mol (i.e., 100% purity) was provided from Sigma-Aldrich (USA), while the solvent ethanol with a molecular weight of 46.07 g/mol (95% purity) was provided from ACP (Canada). The polymer solution was prepared at several concentrations (8, 10, 12, and 16 wt.%) and stirred using magnetic stirrer for 1 hour at room temperature to get homogeneous polymeric solution. The components of the laboratory-scale electrospinning setup are shown in Fig. (1). They include a syringe pump (type NE-300), a 5 mL plastic syringe (23G) sharp-end 23G needle, and a rotation collector. The constructed needle is attached to the positive end of the voltage power supply.

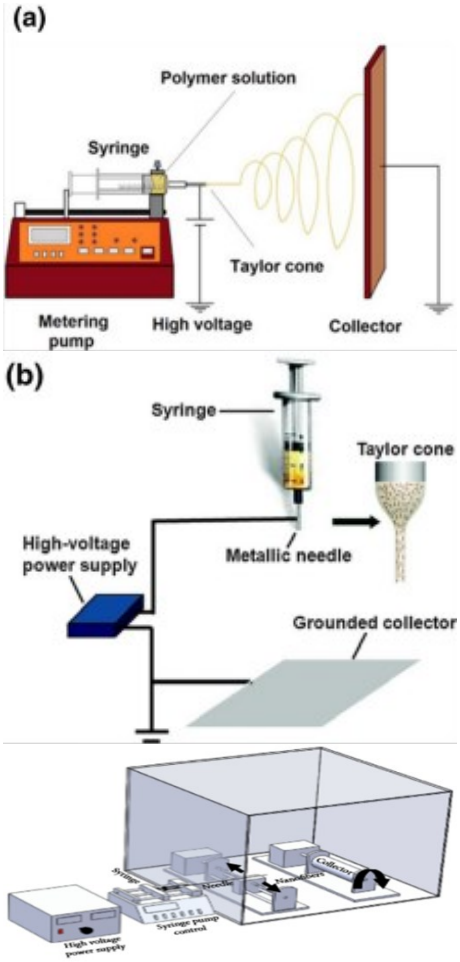

Fig. (1) Electrospinning setup (a) process, (b) schematic, and (c) round collector

3. Results and Discussion

The X-ray diffraction (XRD) measurement was carried out on the PVP nanofibers at ambient temperature around 39°C and relative humidity of approximately 35% in the angle (2θ) range from 10° to 80°. Figure (2) shows the XRD pattern for PVP nanofibers. There are wide peaks between (20-30°), which indicate that the polymer is amorphous [23], while Jie Bai et al found that the peak appeared at 20.558°, corresponding to the peak of PVP [24].

Figure (3) shows the Fourier-transform infrared (FTIR) spectrum of PVP nanofibers in the range 4000-400 cm^{-1}. FTIR is an important tool to investigate functional groups of organic materials structure, where it illustrates the occurrence of interaction between the various constituents according to the induced changes in the vibration modes and the band position. It appears that peaks of the spectrum are found at 1018.34-1288.36 cm^{-1} related to C-N vibrations, 1452.30 cm^{-1} related to C-H bending vibration, 1647.10 cm^{-1} related to C=O stretching vibration, 2956.67 cm^{-1} related to C-H asymmetric stretching vibration, and 3446.56 cm^{-1} related to O-H stretching vibration [25,26].

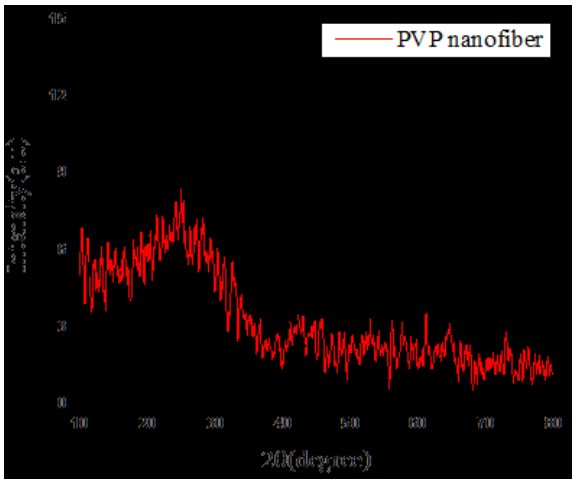

Fig. (2) XRD pattern of PVP nanofibers

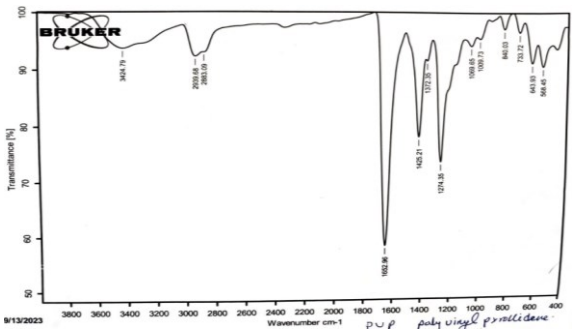

Fig. (3) FTIR spectrum of PVP nanofibers

The morphology of PVP nanofiber was studied using scanning electron microscopy (SEM) whose images are presented the average fiber diameter as shown in table (1). Throughout SEM, the smallest fiber diameter was for sample S3 due to the effect of high applied voltage [27]. As depicted in samples S1, S2, and S3 (Fig. 4), where polymer concentration of 8 wt.%), solution flow rate of 0.9 mL/h, and collector rotation speed of 1200 RPM were kept constant, a progressive increase in applied voltage from 13 to 19 kV resulted in a noticeable decrease in average fiber diameter from 524 nm in S1 to 409 nm in S2, and further down to 379 nm in S3. This behavior can be attributed to the increased electrostatic forces at higher voltages, which intensify the stretching of the polymer jet, ultimately leading to thinner fiber formation. Likewise, in samples S4, S5, and S6 (Fig. 5), where the applied voltage of 10 kV and polymer concentration of 8 wt.% were held constant, increasing the flow rate from 0.6 to 1.2 mL/h resulted in a substantial rise in fiber diameter from 520 nm to 920 nm. This confirms that higher flow rates hinder the stretching and drying processes, promoting the formation of thicker fibers. The effect of polymer concentration was further examined in samples S7, S8, and S9 (Fig. 6), where increasing the PVP content from 10 to 12 wt.%, while maintaining a fixed voltage (10 kV) and rotation speed (1200 RPM), led to a gradual increase in fiber diameters: 847 nm, 924 nm, and 1061 nm, respectively. This trend reflects the rise in solution viscosity at higher concentrations, which enhances molecular entanglements and limits jet elongation, resulting in thicker fibers.

A similar trend was observed in samples S10, S11, and S12 (Fig. 7), fabricated with a constant voltage (10 kV) and increasing polymer concentrations (12 wt.%), where flow rates ranged from 0.6 to 1.2 mL/h. Fiber diameter increased from 538 to 1188 nm, emphasizing the role of both viscosity and polymer chain entanglement in determining fiber thickness.

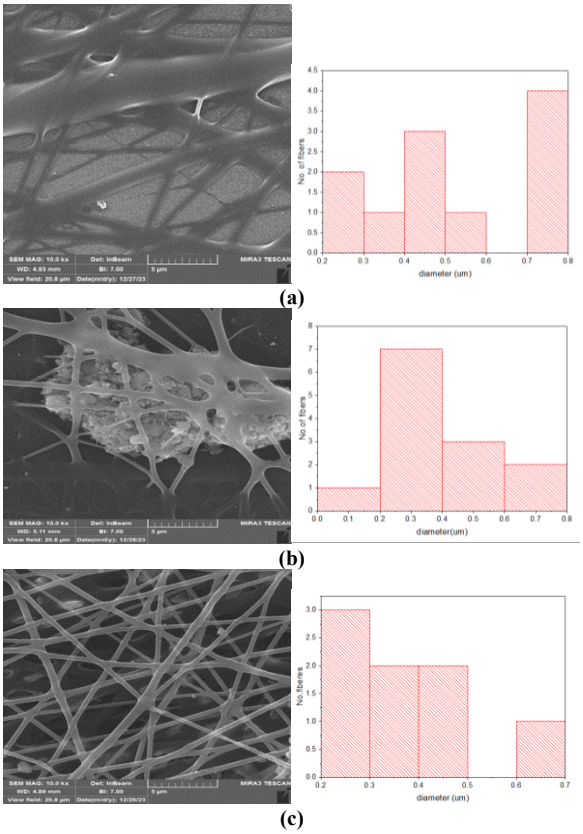

Fig. (4) SEM images and histograms (S1, S2, S3) of different high voltage

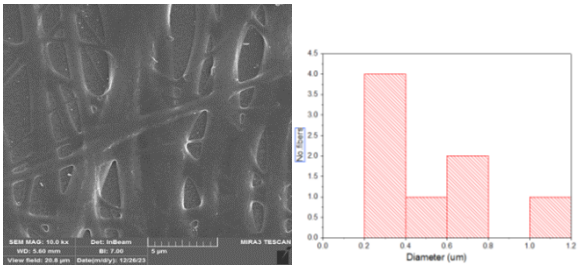

(d)

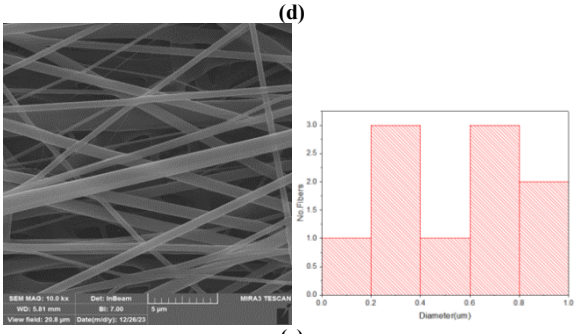

(e)

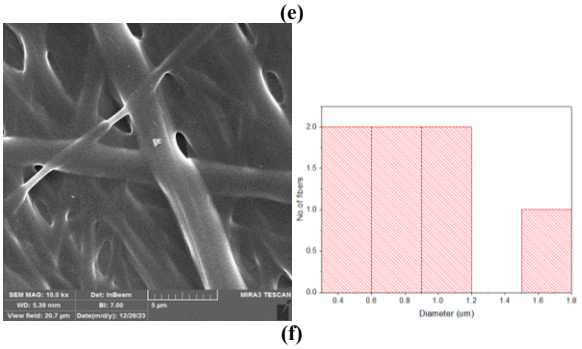

(f)

Fig. (5) SEM images and histograms (S4, S5, S6) at different flow rates

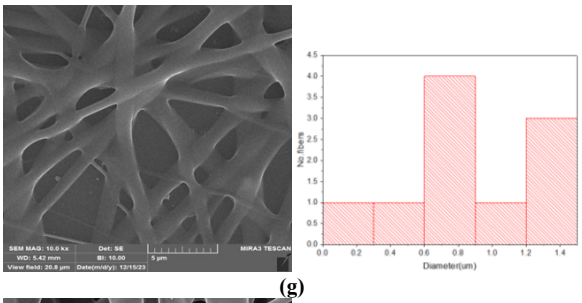

(g)

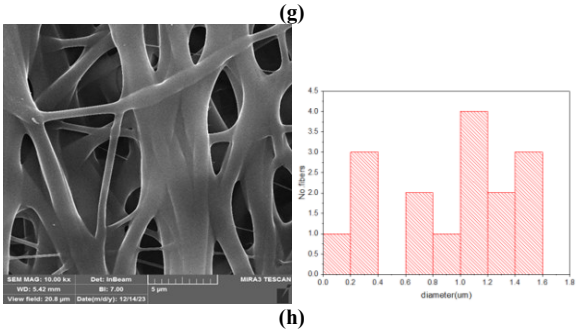

(h)

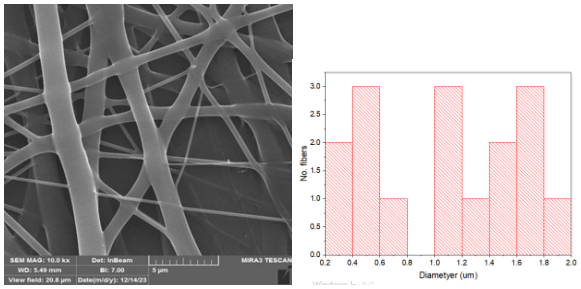

(i)

Fig. (6) SEM images and histograms (S7, S8, S9) of different flow rates

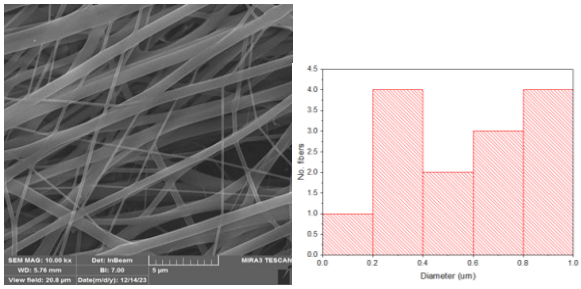

(j)

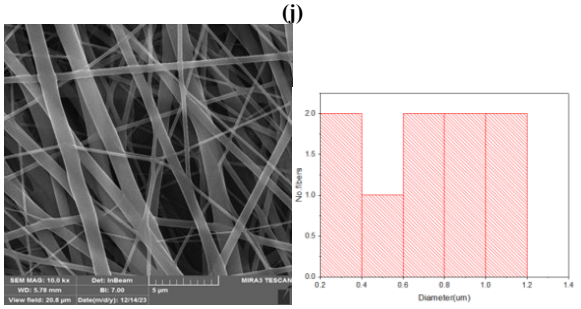

(k)

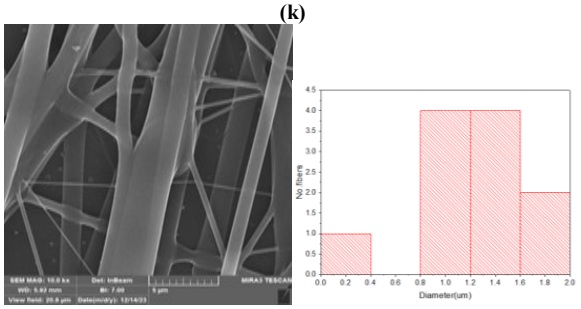

(l)

Fig. (7) SEM images and histograms (S10, S11, S12) at different flow rates

In another set of experiments, samples S13, S14, and S15 (Fig. 8), a higher polymer concentration (16 wt.%) was used while varying the flow rate from 0.3 to 1.0 mL/h under constant voltage. The fiber diameters increased from 560 nm (S13) to 836 nm (S15), indicating that, especially at elevated viscosities, the flow rate significantly affects fiber size. The moderate diameters at lower flow rates (e.g., S13) suggest that a reduced volume of solution allows more time for the jet to stretch and solidify before deposition. Finally, the role of collector rotation speed was investigated using samples S16 through S19 (Fig. 9), where the PVP concentration of 16 wt.%, flow rate of 1.0 mL/h, and

voltage of 10 kV were kept conctant. As the rotation speed was increased from 750 RPM (S19) to 2000 RPM (S18), the fiber diameter decreased markedly from 1121 to 748 nm. This reduction is attributed to enhanced mechanical drawing during deposition, which promotes fiber thinning and alignment. Collectively, the SEM analyses presented in figures 4-9 and summarized in table (1) provide clear evidence of how electrospinning parameters - namely voltage, flow rate, polymer concentration, and collector speed - govern fiber morphology. These experimentally validated trends offer valuable guidance for tailoring PVP nanofibers for applications requiring precise control over fiber dimensions and structural properties.

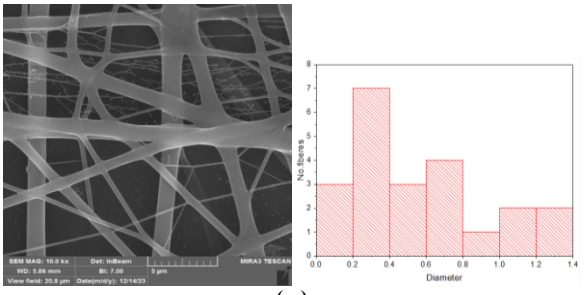

(m)

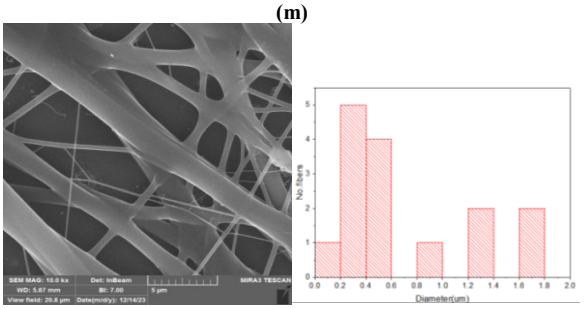

(n)

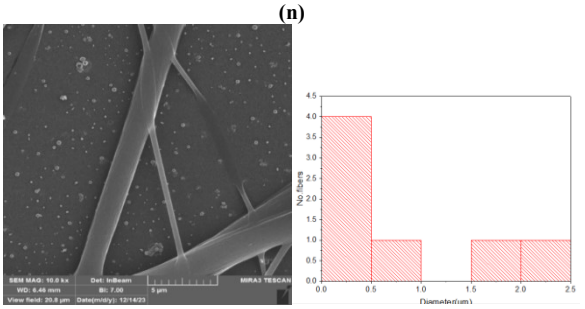

(o)

Fig. (8) SEM images and histograms (S13, S14, S15) at different flow rates

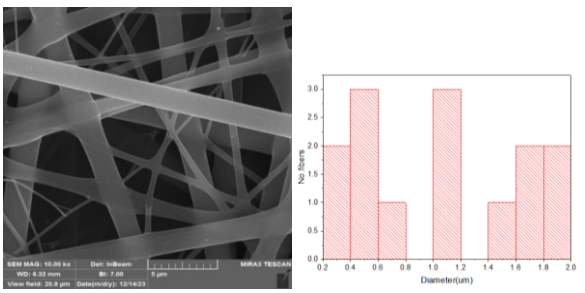

(p)

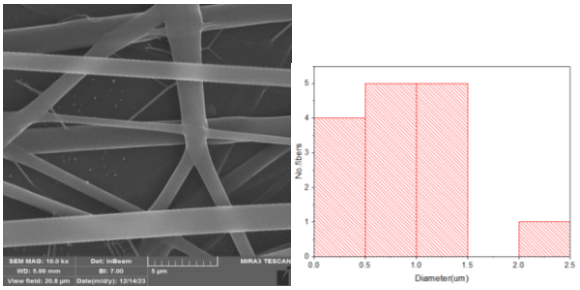

(q)

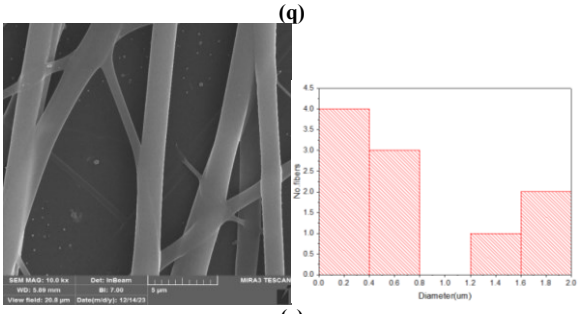

(r)

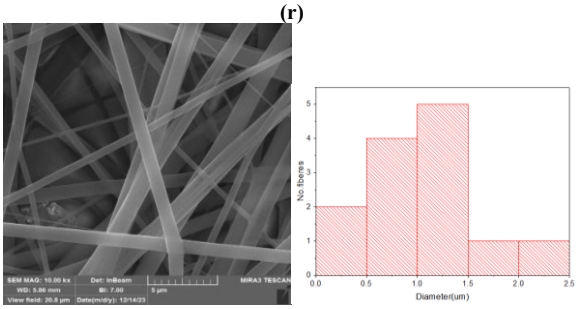

(s)

Fig. (9) SEM images of PVP (16, 17, 18 and 19) at different collector rotation speeds as shown in table (1) at 5µm scale

The thermal analysis of polymers typically employs a combination of advanced techniques, including thermogravimetric analysis (TGA), differential thermal analysis (DTA), differential scanning calorimetry (DSC), and evolved gas analysis (EGA). TGA is specifically utilized to measure weight changes in samples as a function of temperature and time under a controlled atmosphere. The TGA was conducted to evaluate the thermal stability of PVP nanofibers, a critical factor for their potential use in optoelectronic and biomedical fields, where thermal exposure can significantly affect their functional performance This technique is particularly useful for assessing thermal stability, oxidative resistance, and compositional characteristics, such as the presence of fillers, polymer resins, and solvents within the sample. In this research, TGA was performed for PVP powder and PVP fiber, as shown in Fig. (10), while the thermal parameter was listed in table (2).

It was noted from the results the rate of decomposition of the PVP fiber less than PVP powder, this means that the convert the polymer to its fiber leads to more thermal stable than polymer alone, also the decomposition was 420 °C, which higher than PVP alone. On the other hand, the two samples has one

decomposition temperature and very stable still at nearly 400 °C. The enhanced thermal stability observed in electrospun PVP nanofibers, relative to the untreated powder form, can be ascribed to multiple underlying factors. The high-voltage stretching inherent to the electrospinning process promotes improved molecular orientation, which may contribute to increased thermal resistance. Furthermore, although PVP is generally considered an amorphous polymer, the rapid evaporation of solvent during fiber formation may induce regions of localized order or semi-crystallinity, potentially raising the decomposition threshold. Additionally, the continuous fibrous morphology exhibits a reduced surface area relative to the bulk powder, thereby minimizing susceptibility to thermal oxidation and improving overall thermal durability [28]

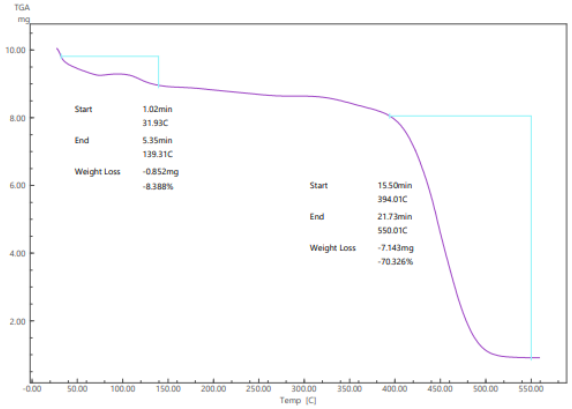

(a)

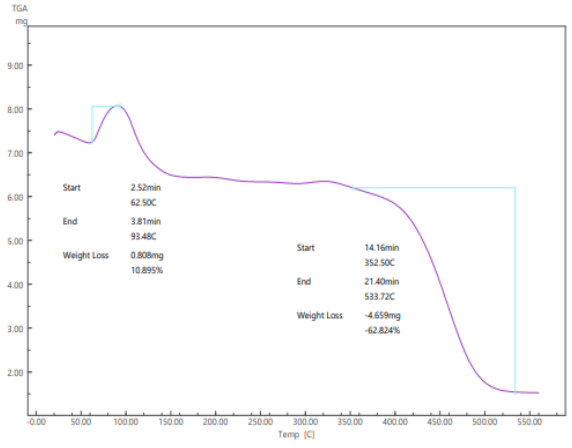

(b)

Fig. (10) TGA thermograms of PVP (a) powder (b) fiber

The absorption spectrum of the PVP nanofiber of sample S3 (due to its smallest fiber diameter) (Fig. 11) exhibits a sharp edge in the UV region at 300 nm, which is attributed to the n→π* transition [22]. Additionally, the films demonstrate low absorption in the longer wavelength region [29]. The reflectance can be roughly calculated from the relation [30]:

$$A + T + R = 1 \qquad (1)$$

Figure (12) presents the transmission and reflection spectra. It is observed that transmittance increases with wavelength, which can be attributed to the weak absorption in the region beyond 350 nm. The reflectance spectrum exhibits a maximum value at a wavelength of 309 nm, reaching approximately 23%.

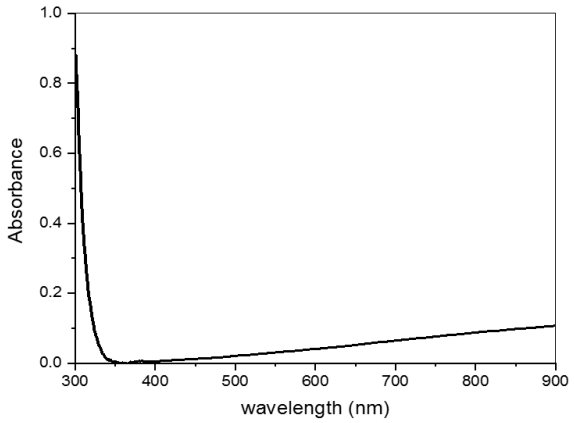

Fig. (11) Relation between absorbance and wavelength of PVP nanofibers

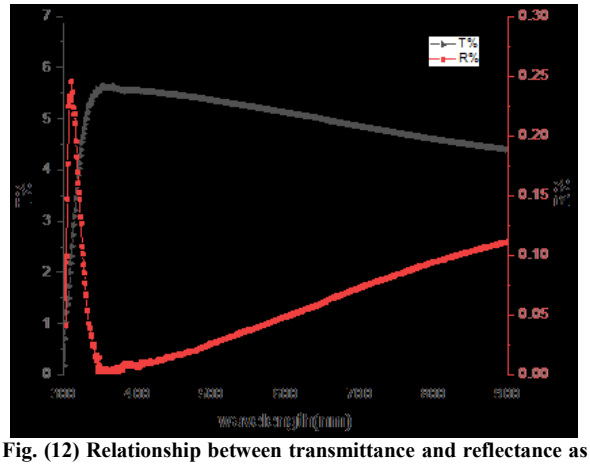

Fig. (12) Relationship between transmittance and reflectance as a function of wavelength for PVP nanofibers

The optical absorption coefficient (α) can be determined using the following equation [27]:

$$\alpha = \frac{2.303\ log\ (\frac{1}{T})}{d} \qquad (2)$$

where d denotes the film thickness. Figure (13) displays the relationship between the absorption coefficient (α) and photon energy (hν) within the energy range of 1–5 eV for the PVP nanofiber film.

The extinction coefficient (k) for the PVP nanofiber film was determined from the absorption coefficient values using the following equation [23]:

$$k = \frac{\alpha\lambda}{4\pi} \qquad (3)$$

As observed, the extinction coefficient (k) decreases with increasing wavelength due to the low absorption in the longer wavelength region, similar to the behavior of the absorption coefficient (α). The value of k is approximately 0.048 at 301 nm.

The refractive index (n) can be determined using the following equation [29]:

$$n = \left(\frac{1+\sqrt{R}}{1-\sqrt{R}}\right) \quad (4)$$

The refractive index (n) exhibits high values in the wavelength range of 300–350 nm, which can be attributed to the reduction in light speed within this region. In contrast, for wavelengths longer than 400 nm, the refractive index gradually decreases. The maximum recorded value of n is approximately 2.96 at 311 nm.

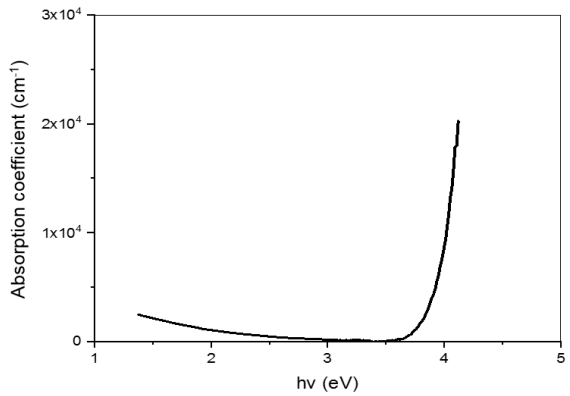

Fig. (13) Relationship between the absorption coefficient (α) and photon energy (hν) for PVP nanofibers

The optical energy gap (E_g) of PVP nanofiber films is determined using Tauc's relation [31]:

$$\alpha h\nu = A(h\nu - E_g)^r \quad (5)$$

where $h\nu$ represents the energy of the incident photon, A is the transition probability parameter, and r denotes the nature of the electronic transition. Given that the absorption coefficient (α) is $\geq 10^4$ cm^{-1}, the transition type is identified as an allowed indirect transition. Figure (14) illustrates the relationship between $(\alpha h\nu)^2$ and photon energy (hν). From this figure, the linear fit in the high-energy region is used to determine the optical energy gap (E_g), which is found to be 3.98 eV for PVP. Ahmed et al. [31] have previously reported an E_g value of approximately 4 eV for PVP, confirming the dielectric nature of this material.

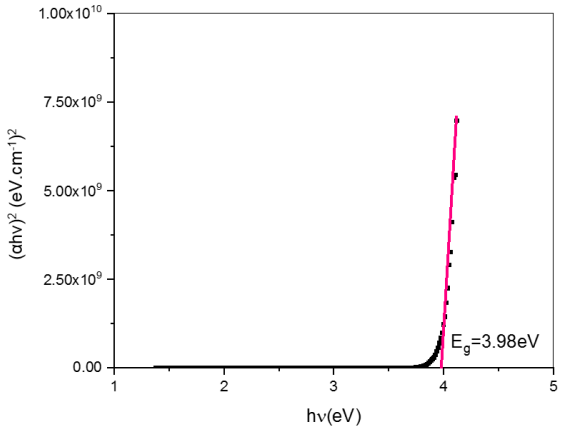

Fig. (14) Relation of $(\alpha h\upsilon)^2$ as a function of photon energy (hυ) of PVP nanofiber

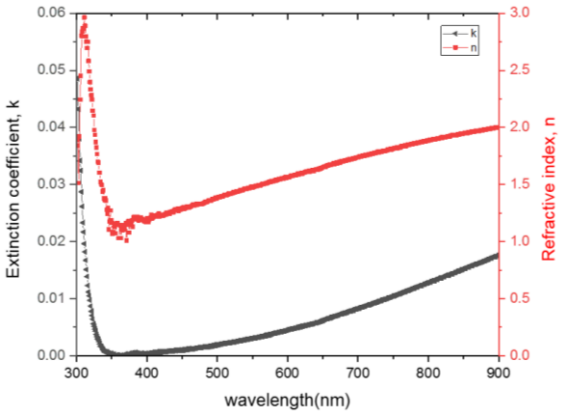

Fig. (15) The excitation coefficient (k) and refractive index (n) as functions of wavelength

4. Conclusions

In this work, PVP nanofibers were fabricated by electrospinning with a detailed evaluation of how key operational variables affect fiber morphology. The experimental findings revealed that increasing the electric field intensity and decreasing the flow rate led to a noticeable reduction in fiber diameter. Conversely, higher concentrations of polymer and slower rotation resulted in the formation of thicker fibers. These observations underscore the necessity of carefully tuning electrospinning parameters to achieve desired fiber size and uniformity. Enhanced thermal stability in the electrospun fibers was demonstrated compared to pristine PVP, indicating their suitability for thermally demanding applications. The calculated optical band gap was approximately 3.98 eV, confirming its dielectric behavior and relevance for use in optoelectronic devices. In summary, this study offers valuable insights into how electrospinning parameters can be manipulated to tailor the structural, thermal, and optical features of PVP nanofibers.

References

[1] W.E. Teo and S. Ramakrishna, "A review on electrospinning design and nanofibre assemblies", *Nanotech.*, 17 (2006) R89.

[2] F.E. Ahmed, B.S. Lalia and R. Hashaikeh, "A review on electrospinning for membrane fabrication: Challenges and applications", *Desalinat.*, 356 (2015) 15-30.

[3] J. Doshi and D.H. Reneker, "Electrospinning process and applications of electrospun fibers", *J. Electrostat.*, 35 (1995) 151-160.

[4] W. Lu, J. Sun and X. Jiang, "Recent advances in electrospinning technology and biomedical applications of electrospun fibers", *J. Mater. Chem. B*, 2 (2014) 2369-2380.

[5] R. Asmatulu et al., "Nanofiber fabrication and characterization for the engineering education", in Proceedings of the 2007 ASEE Midwest Regional Conference (2007), pp. 19-21.

[6] A. Haghi and M. Akbari, "Trends in electrospinning of natural nanofibers", *phys. stat. sol. (a)*, 204 (2007) 1830-1834.
[7] M. Ziabari, V. Mottaghitalab and A. Haghi, "Application of direct tracking method for measuring electrospun nanofiber diameter", *Brazilian J. Chem. Eng.*, 26 (2009) 53-62.
[8] Z. Li and C. Wang, **"One-dimensional Nanostructures: Electrospinning Technique and Unique Nanofibers"**, Springer (2013).
[9] C. Thompson et al., "Effects of parameters on nanofiber diameter determined from electrospinning model", *Polymer*, 48 (2007) 6913-6922.
[10] J. Tao and S. Shivkumar, "Molecular weight dependent structural regimes during the electrospinning of PVA", *Mater. Lett.*, 61 (2007) 2325-2328.
[11] J.M. Deitzel et al., "The effect of processing variables on the morphology of electrospun nanofibers and textiles", *Polymer*, 42 (2001) 261-272.
[12] A. Koski, K. Yim and S. Shivkumar, "Effect of molecular weight on fibrous PVA produced by electrospinning", *Mater. Lett.*, 58 (2004) 493-497.
[13] D.H. Reneker and I. Chun, "Nanometre diameter fibres of polymer, produced by electrospinning", *Nanotech.*, 7 (1996) 216.
[14] C. Zhang et al., "Study on morphology of electrospun poly (vinyl alcohol) mats", *Euro. Polym. J.*, 41 (2005) 423-432.
[15] X. Yuan et al., "Morphology of ultrafine polysulfone fibers prepared by electrospinning", *Polym. Int.*, 53 (2004) 1704-1710.
[16] D.S. Katti et al., "Bioresorbable nanofiber-based systems for wound healing and drug delivery: Optimization of fabrication parameters", *J. Biomed. Mater. Res. B: Appl. Biomater.*, 70 (2004) 286-296.
[17] J.S. Lee et al., "Role of molecular weight of atactic poly (vinyl alcohol)(PVA) in the structure and properties of PVA nanofabric prepared by electrospinning", *J. Appl. Polym. Sci.*, 93 (2004) 1638-1646.
[18] C.J. Buchko et al., "Processing and microstructural characterization of porous biocompatible protein polymer thin films", *Polymer*, 40 (1999) 7397-7407.
[19] S. Zhao et al., "Electrospinning of ethyl–cyanoethyl cellulose/tetrahydrofuran solutions", *J. Appl. Polym. Sci.*, 91 (2004) 242-246.
[20] N. Li, J. Xiong and H. Xue, "Effect of wheel rotating speed and LiCl additives on electrospun aligned polyacrylonitrile nanofiber", *Polym. Eng. Sci.*, 51 (2011) 2178-2183.
[21] N. Bhardwaj and S.C. Kundu, "Electrospinning: A fascinating fiber fabrication technique", *Biotech. Adv.*, 28 (2010) 325-347.
[22] Q.P. Pham, U. Sharma and A.G. Mikos, "Electrospinning of polymeric nanofibers for tissue engineering applications: a review", *Tissue Eng.*, 12 (2006) 1197-1211.
[23] Y.-N. Jiang, H.-Y. Mo and D.-G. Yu, "Electrospun drug-loaded core–sheath PVP/zein nanofibers for biphasic drug release", *Int. J. Pharmaceut.*, 438 (2012) 232-239.
[24] J. Bai et al., "Electrospinning method for the preparation of silver chloride nanoparticles in PVP nanofiber", *Appl. Surf. Sci.*, 254 (2008) 4520-4523.
[25] H. Liu et al., "Hydrothermal synthesis of monodisperse Ag_2Se nanoparticles in the presence of PVP and KI and their application as oligonucleotide labels", *J. Mater. Chem.*, 18 (2008) 2573-2580.
[26] S. Selvam and M. Sundrarajan, "Functionalization of cotton fabric with PVP/ZnO nanoparticles for improved reactive dyeability and antibacterial activity", *Carbohyd. Polym.*, 87 (2012) 1419-1424.
[27] H. Utkarsh et al., "Towards analysis and optimization of electrospun PVP (polyvinylpyrrolidone) nanofibers", *Adv. Polym. Technol.*, 2020 (2020) 4090747.
[28] Y. Cho et al., "Electrospinning and nanofiber technology: fundamentals, innovations, and applications", *Adv. Mater.*, (2025) 2500162.
[29] T. Tański, W. Matysiak and Ł. Krzemiński, "Analysis of optical properties of TiO_2 nanoparticles and PAN/TiO_2 composite nanofibers", *Mater. Manufact. Process.*, 32 (2017) 1218-1224.
[30] E.D. Boland et al., "Tailoring tissue engineering scaffolds using electrostatic processing techniques: a study of poly (glycolic acid) electrospinning", *J. Macromol. Sci. A*, 38 (2001) 1231-1243.
[31] R. Ahmed, N. Hassan and I. Ibrahim, "The structural and figure of merit photodetector of PVP-doped with lanthanum", *Digest J. Nanomater. Biostruct.*, 17 (2022).

Table (1) Parameters used of electro spinning at constant collecting distance, deposition time and ambient conditions

Sample	Flow rate (mL/h)	Applied voltage (kV)	Concentration (wt.%)	Rotation speed RPM	Average diameter (nm)
1	0.9	13	8	1200	524
2	0.9	16	8	1200	409
3	0.9	19	8	1200	379
4	0.6	10	8	1200	520
5	0.9	10	8	1200	541
6	1.2	10	8	1200	920
7	0.6	10	10	1200	847
8	1	10	10	1200	924
9	1.2	10	10	1200	1061
10	0.6	10	12	1200	538
11	0.9	10	12	1200	743
12	1.2	10	12	1200	1188
13	0.3	10	16	1200	560
14	0.6	10	16	1200	712
15	1	10	16	1200	836
16	1	10	16	1200	1042
17	1	10	16	1600	866
18	1	10	16	2000	748
19	1	10	16	750	1121

Table (2) Thermal parameter evaluated from TGA thermograms

Sample	Decomposition Rate (%\min.)	Decomposition Temperature (°C)	Char residue at 500°C (%)	Temperature of 25wt.% loss	Temperature of 50wt.% loss	Temperature of 75wt.% loss
PVP-powder	9.38	416	22	418	457	475
PVP fiber	4.43	420	27	420	450	471

